Electrocatalysis
DOI 10.1007/s12678-016-0345-7

ORIGINAL RESEARCH

Facile Synthesis of Cobalt Oxide Nanoparticles by Thermal Decomposition of Cobalt(II) Carboxamide Complexes: Application as Oxygen Evolution Reaction Electrocatalyst in Alkaline Water Electrolysis

Soraia Meghdadi[1] · **Mehdi Amirnasr**[1] · **Mohammad Zhiani**[1] · **Fariba Jallili**[1] · **Meysam Jari**[1] · **Mahsa Kiani**[1]

© Springer Science+Business Media New York 2016

Abstract Cobalt oxide nanoparticles, Co_3O_4 (**1**) and Co_3O_4 (**2**), have been synthesized by thermal decomposition of [Co^{II}(bqbenzo)] and [Co^{II}(bqb)], respectively. The morphology of these oxides is influenced by the difference in the structure of bqbenzo^{2-} {3,4-bis(2-quinolinecarboxamido) benzophenone and, bqb^{2-} {bis(2-quinolinecarboxamido)-1,2-benzen}, only differing in a benzoyl substituent. The products were characterized by XRD, FE-SEM, and FT-IR spectroscopy. The catalytic activity of the oxides was examined in oxygen evolution reaction (OER) by cyclic voltammetry (CV) and linear sweep voltammetry (LSV). The Co_3O_4 oxides (**1** and **2**) exhibited higher catalytic activity compared to 10 wt% Pt/C in terms of obtained current density at 0.8 V; ~23.3 versus 6.1 mA cm^{-2}, respectively. However, the aging tests of the two oxides in OER revealed that Co_3O_4 (**1**) is more stable than Co_3O_4 (**2**). These results demonstrated that the Co_3O_4 (**1**) has a superior performance which can be employed in the alkaline water electrolyzer anode.

Keywords Cobalt carboxamide complex · Co_3O_4 nanoparticles · Oxygen evolution reaction · Water oxidation · Anode catalyst

Electronic supplementary material The online version of this article (doi:10.1007/s12678-016-0345-7) contains supplementary material, which is available to authorized users.

✉ Soraia Meghdadi
smeghdad@cc.iut.ac.ir

✉ Mehdi Amirnasr
amirnasr@cc.iut.ac.ir

[1] Department of Chemistry, Isfahan University of Technology, Isfahan 8415683111, Iran

Introduction

Electrocatalytic transformation of water to H_2 and O_2 has attracted increasing attention for producing clean energy and efficient energy storage [1–3]. The oxygen evolution reaction (OER, $4H^+/4e^-$), which requires a large overpotential, is one of the major scientific challenges in this transformation [4–6]. Although, the oxides of some noble metals such as Ru and Ir exhibit excellent activity towards OER [7–9], it is highly desired to search for efficient and low-cost OER catalysts to reduce the overpotential and enhance the current density.

In recent years, tremendous efforts have been dedicated to searching for inexpensive OER electrocatalyts. Amongst the most promising materials that have displayed a combination of desired stability, relatively low overpotential, and viable cost are various transition metals and metal oxides, including cobalt oxides [10–12] and nickel oxides prepared by different methods [13–15]. To get a better performance however, cobalt oxide nanoparticles have been used to fabricate metal oxide-based electrodes. These nanoparticles are prepared by a variety of synthetic methods using different precursors, including thermal decomposition of suitable cobalt coordination compounds [16]. In this context, several cobalt complexes such as $Co(C_6H_5COO)_2(N_2H_4)_2$ [17] and $[(NH_3)_5Co(O_2)Co(NH_3)_5](NO_3)_4$ [18] have been used for the synthesis of Co_3O_4 NPs by thermal decomposition. However, more convenient and benign synthesis of the precursors from readily available reagents is highly desirable.

Pyridine carboxamide ligands and their metal complexes are amongst the well distinguished and available compounds that are very attractive to inorganic chemists due to their diverse applications. These compounds have exhibited extraordinary properties and have been exploited in a great variety of catalytic and biological

Published online: 10 December 2016

process [19–25]. One factor that makes carboxamides attractive for different applications is the simplicity of the structural modification of these ligands by a modular approach. The steric and electronic properties can conveniently be modified by altering the pyridine carboxylic acid or the diamine backbone via introducing suitable substituents to the rings [26–30]. These modifications will presumably fine-tune the structures and properties of their metal complexes that may serve as precursors for the synthesis of metal oxide nanoparticles.

In this context, herein, we report the synthesis of H_2bqbenzo and H_2bqb ligands by a benign and efficient method that we have recently developed in our laboratory for the synthesis of carboxamide derivatives [28–31]. The synthesis of the corresponding cobalt(II) complexes, [Co^{II}(bqbenzo)] and [Co^{II}(bqb)], and preparation of Co_3O_4 nanoparticles **1** and **2** by thermal decomposition of these precursors are also presented. The effect of benzoyl substituent on the final morphology of Co_3O_4 nanoparticles and the application of these NPs for electrocatalytic water oxidation are also reported and discussed.

Experimental

Materials and Methods

All solvents and chemicals were of commercial reagent grade and used as received from Aldrich and Merck. Elemental analyses were performed using a Perkin–Elmer 2400II CHNS-O elemental analyzer. UV-Vis spectra were recorded on a JASCO V-570 spectrophotometer. Infrared spectra (KBr pellets) were obtained on a FT-IR JASCO 680 plus spectrophotometer. The 1 H NMR spectra of the ligands were obtained on a BRUKER AVANCE DR (500 MHz) and BRUKER AVANCE III (400 MHz) spectrometer. Proton chemical shifts are reported in parts per million (ppm) relative to an internal standard of Me_4Si. Thermogravimetric analyses (TGA) were carried out using a thermogravimetric analysis instrument (BAHR STA-503) in air and a heating rate of 10 °C min^{-1}. The XRD patterns were recorded by a Philips X-pert MPD X-ray diffractometer using Ni-filtered Cu Kα radiation with voltage of 40 kV in the range of 20–80° for 2 theta (2). Scanning electron microscopy (SEM) images were obtained using a MIRA3 TESCAN device.

Electrochemical measurements were carried out using a potentiostat/galvanostat (SAMA 500). A commercial glassy carbon GC electrode was used as a working electrode with π mm^2 surface area. An Ag/AgCl (sat'd KCl) and Pt plate were used as the reference and the counter electrodes, respectively.

Synthesis of the Asymmetric Carboxamid Ligand, H_2bqbenzo (L^1)

A mixture of 3.1 g (10 mmol) triphenylphosphite (TPP), 1.61 g (5 mmol) tetrabutylammonium bromide (TBAB), 1.73 g (10 mmol) quinaldic acid, and 1.06 g (5 mmol) 3,4-diaminobanzophenon in a 25-mL round bottom flask was placed in an oil bath (Scheme 1). The reaction mixture was heated until a homogeneous solution was formed. The solution was stirred for 55 min at 120 °C. The viscous solution was cooled to room temperature and then treated with 20 mL cold methanol. The resulting light cream solid was filtered-off and washed with cold methanol. Yield (64%). Anal. Calcd. for $C_{33}H_{22}N_4O_3$ (522.55 g mol^{-1}): C, 75.85; H, 4.24; N, 10.72. Found: C, 74.72; H, 4.22; N, 10.73%. FT-IR (KBr, cm^{-1}) ν_{max}: 3330 (s, N–H), 1696 (s, C = O_{amidic}), 1647 (s, C = O_{benzo}), 1588 (s, C = C), 1529 (s, C–N). ^{1}H NMR (400 MHz, $CDCl_3$, 298 K): δ (ppm) = 7.54–8.53 (20H, ArH), 10.56 (S, 1H, NH), 11.07 (S, 1H, NH).

Synthesis of the Symmetric Carboxamide Ligand H_2bqb (L^2)

This ligand was prepared according to the procedure used for H_2bqbbenzo except that o-phenylenediamine was used instead of 3,4-diaminobanzophenon (Scheme 1). The resulting light cream solid was filtered-off and washed with cold methanol. Yield (90%). Anal. Calcd. for $C_{26}H_{18}N_4O_2$ (418.45 g mol^{-1}): C, 74.63; H, 4.34; N, 13.39. Found: C, 74.45; H, 4.34; N, 13.37%. FT-IR (KBr, cm^{-1}): ν_{max} = 3320 (s, NH), 1690 (s, C = O_{amidic}),1590 (s, C = C), 1530 (s, C–N); ^{1}H NMR (500 MHz, $CDCl_3$, 298 K): δ(ppm) = 7.37–8.54 (12H, ArH), 10.61 (s, 1H, NH).

Synthesis of [Co^{II}(bqbenzo)]

A solution of 1.57 g (0.003 mol) of H_2bqbenzo in 50 mL chloroform was added dropwise to a solution of 0.747 g (0.003 mol) of cobalt(II) acetate tetrahydrate in 50 mL methanol. The resulting red solution was left undisturbed at room temperature for 4 days to give red crystals of Co^{II}(bqbenzo). The crystals were isolated by filtration, washed with cold methanol, and dried in vacuum. Yield: 91%. Anal. Calcd. for $C_{33}H_{20}CoN_4O_3$ (579.47 g mol^{-1}): C, 68.40; H, 3.48; N, 9.67. Found: C, 67.73; H, 3.42; N, 9.56%. FT-IR (KBr, cm^{-1}): ν_{max} = 1650 (s, C = O_{amidic}), 1617 (s, C = O_{benzo}), 1594 (s, C = C), 1568 (s, C–N).

Synthesis of [Co^{II}(Bqb)]

A solution of 1.26 g (0.003 mol) of H_2bqb in 50 mL chloroform was added dropwise to a solution of 0.747 g (0.003 mol) of cobalt(II) acetate tetrahydrate in 50 mL

Scheme 1 Synthesis of carboxamide ligands H_2bqbenzo ($\mathbf{L^1}$) and H_2bqb ($\mathbf{L^2}$)

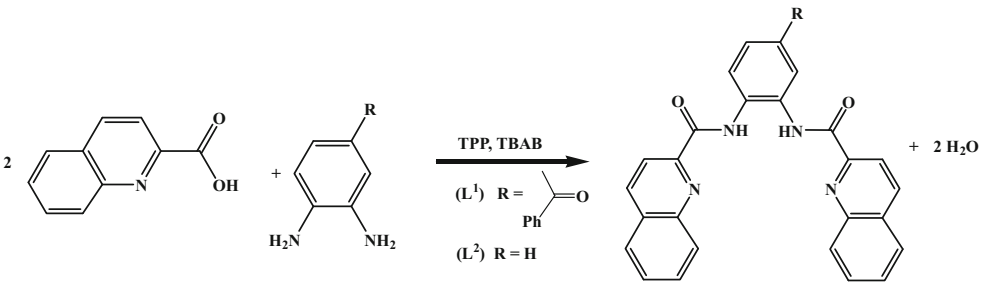

methanol. The resulting red orange solution was left undisturbed at room temperature for 4 days to give red orange crystals of Co^{II}(bqb). The crystals were isolated by filtration, washed with cold methanol, and dried in vacuum. Yield: 91%. Anal. Calcd. for $C_{26}H_{16}CoN_4O_2$ (475.36 g mol^{-1}): C, 65.69; H, 3.39; N, 11.79. Found: C, 65.83; H, 3.42; N, 11.66%. FT-IR (KBr, cm^{-1}): ν_{max} = 1665 (s, C = O_{amidic}), 1590 (s, C = C), 1540 (s, C–N).

Synthesis of Co_3O_4 Nanoparticles

The Co_3O_4 nanoparticles (**1**) and (**2**) were synthesized by thermal decomposition of [Co^{II}(bqbenzo)] or [Co^{II}(bqb)], respectively. The calcination temperature for each complex was determined based on TG-DTA results (*vide infra*). Each cobalt complex was grinded and placed in a pre-dried ceramic crucible. The crucible was heated in a furnace set at 500 °C for 2 h in the presence of air. The sample was then cooled to room temperature and the black Co_3O_4 nanocrystals were collected and characterized by FT-IR, XRD, and FE-SEM.

Electrochemical Measurements

The experiments were carried out in solutions containing 1 M KOH at room temperature. The catalytic activity of the catalysts were tested using cyclic voltammetry (CV) at a scan rate of 50 mV s^{-1} and linear sweep voltammetry (LSV) at a scan rate of 5 mV s^{-1}. The working electrode was prepared by the following steps: (i) the catalyst (2 mg) was dispersed in isopropanol-H_2O (*v*/*v* = 80:20, 300 μL) solution containing a small amount of 2 wt%. Nafion solution to form a homogeneous mixture under sonication, and (ii) 1 μL of the ink solution was transferred onto the surface of the GC by micro pipette. After drying the electrode at 60 °C in an oven, the catalyst loading of oxides was 0.2 mg cm^{-2}. In the case of Pt/C, metal loading of the electrode was 0.2 mg_{Pt} cm^{-2}.

Results and Discussion

Infrared Spectroscopic Analysis

Figure 1a shows the FT-IR spectrum of [Co^{II}(bqbenzo)]. This complex exhibits four vibrational bands at 1650, 1617, 1594, 1568 cm^{-1}, characteristic of ν(C = O_{amidic}), ν(C = O_{benzo}), ν(C = C), ν(C–N), respectively. Figure 1c shows the FT-IR spectrum of [Co(bqb)]. This complex exhibits three vibrational bands at 1665, 1590, and 1540 cm^{-1} and characteristic of ν(C = O_{amidic}), ν(C = C), ν(C–N) respectively. In the FT-IR spectra of the calcination products, presented in Fig. 1b, d, no relevant peaks indicating the presence of organic ligands or fragments are observed. However, the appearance of two strong bands in the FT-IR spectra of the thermal decomposition products of both precursor complexes, (at 664 and

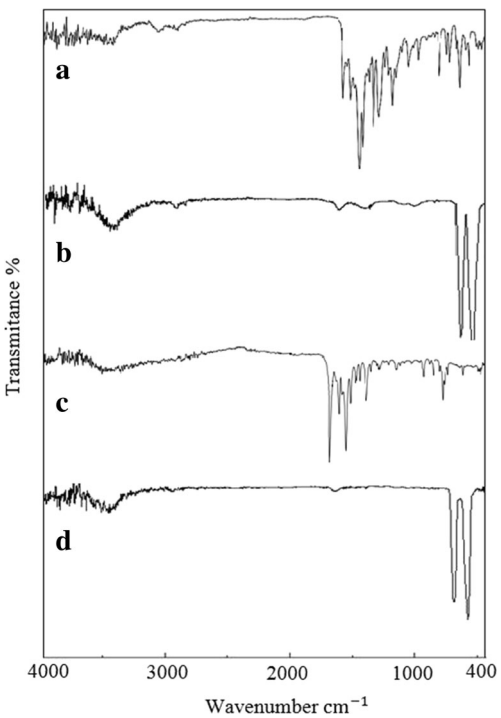

Fig. 1 FT-IR spectra of (*a*) [Co^{II}(bqbenzo)], (*b*) Co_3O_4(**1**), (*c*) [Co^{II}(bqb)], (*d*) Co_3O_4(**2**)

571 cm^{-1} for **1**, and 679 and 562 cm^{-1} for **2**) confirms the spinel structure of Co_3O_4 as the decomposition product.

The peak appearing at 664 cm^{-1} in Fig. 1b and at 679 cm^{-1} in Fig. 1d is attributed to the M–O bond stretching mode, in which M is Co^{2+} and is tetrahedrally coordinated. The band at 571 cm^{-1} in Fig. 1b and at 562 cm^{-1} in Fig. 1d can be assigned to the M–O stretching vibration, with M as the octahedrally coordinated Co^{3+} [32, 33]. The broad band at about 3450 cm^{-1} is assigned to the adsorbed water.

Thermogravimetric Analysis

Figure 2a shows the thermogram of [Co^{II}(bqbenzo)] precursor indicating that the compound is relatively stable until it

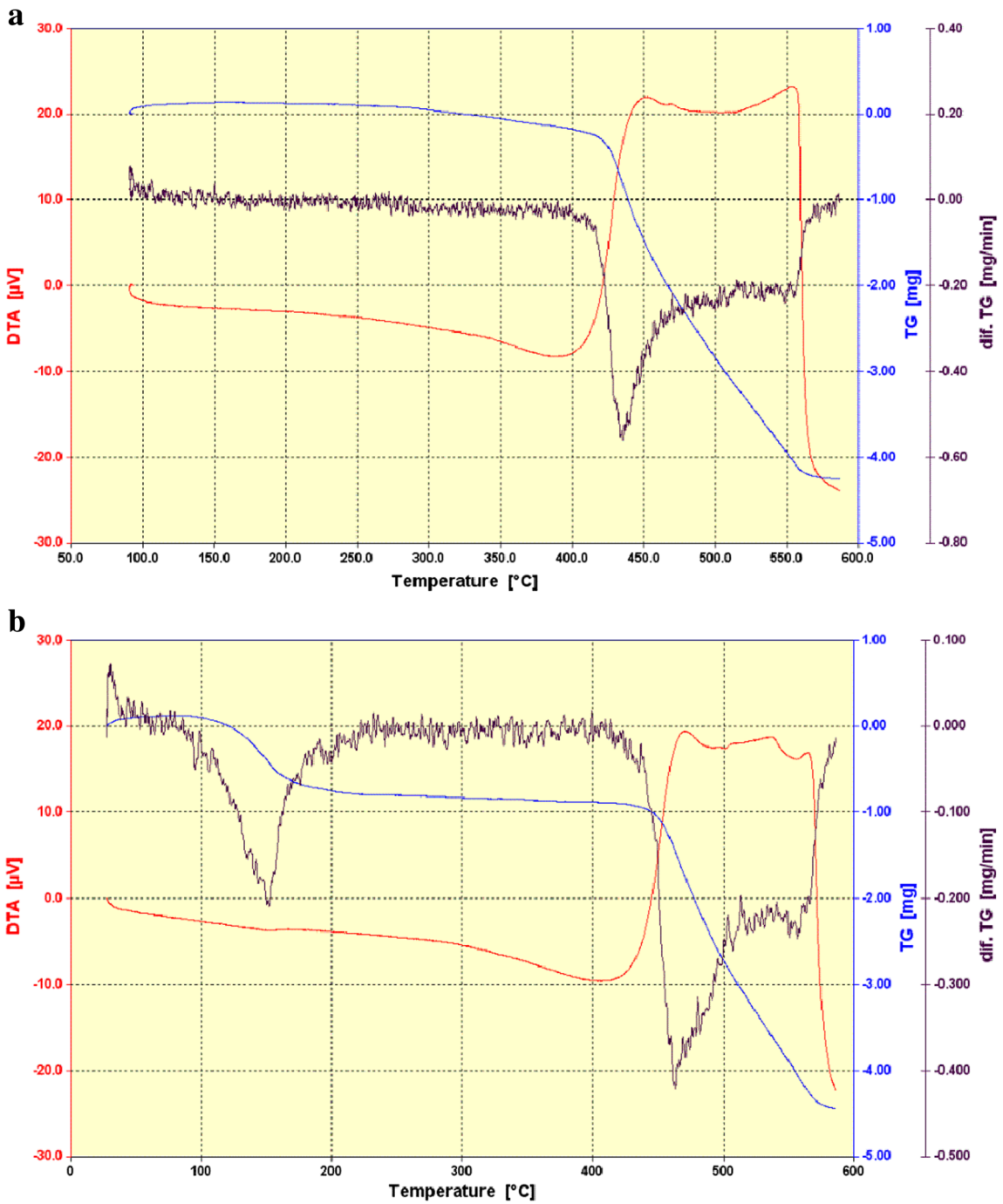

Fig. 2 **a** TGA, DTG, and DTA thermograms of precursor [Co^{II}(bqbenzo)] in air atmosphere. **b** TGA, DTG, and DTA thermograms of precursor [Co^{II}(bqb)] in air atmosphere

reaches the temperature of 420 °C where decomposition of the ligand starts. A significant mass change (found 82.5%, cacl. 86.1%) occurs in the range of 420 to 560 °C (peak centered at 434 °C) corresponding to the decomposition of the ligand, and the cobalt oxide Co_3O_4 (**1**) is finally produced.

Figure 2b shows the thermogram of [Co^{II}(bqb)] precursor indicating the decomposition of the ligand in two steps. Complete decomposition of the ligand with a significant change in the mass (found 81.5%, cacl. 83.1%) occurs in the temperature range of 450 to 560 °C (peak centered at 462 °C), and cobalt oxide Co_3O_4 (**2**) is finally produced. The structure of Co_3O_4 is confirmed by FT-IR and XRD.

X-ray Diffraction Analysis

The XRD pattern of Co_3O_4(**1**) obtained from the thermal decomposition of the [Co^{II}(bqbenzo)] complex at 500 °C for 2 h is shown in Fig. 3a The well-defined diffraction pattern indicates that the sample is crystalline. The XRD pattern shows diffraction peaks with 2θ values of 31.48, 37.04, 38.78, 45.04, 55.88, 59.57, 65.47, and 77.57° that are assigned to the (220), (311), (222), (400), (422), (511), (440), and (533) crystal planes of the crystalline Co_3O_4 phase, respectively and are in good agreement with the JCPDS file of the cubic spinel-type Co_3O_4 phase (JCPDS Card No. 74-1656). The XRD pattern of Co_3O_4 (**2**) obtained from thermal decomposition of [Co^{II}(bqb)] precursor (Fig. 3b) exhibits diffraction peaks with 2θ values of 31.31, 36.88, 38.55, 44.77, 55.73, 59.55, 65.26, 68.77, 77.39, and 78.55° that are assigned to the (220), (311), (222), (400), (422), (511), (400), (531), (533), and (622) crystal planes of the crystalline Co_3O_4 phase, respectively. All the diffraction peaks are in good agreement with the JCPDS file of the cubic spinel-type Co_3O_4 phase (JCPDS Card No. 42-1467). These results confirm that the complex is decomposed completely into the Co_3O_4 phase at 500 °C, in good agreement with the TG-DTA and FT-IR results.

The crystallite size of the as synthesized product, D_c, was calculated from the average of the major diffraction peaks using the Scherrer formula (Eq.(1)) [34] :

$$D_c = \frac{K\lambda}{\beta\cos\theta} \quad (1)$$

where K is a constant (ca. 0.9); λ is the X-ray wavelength used in XRD (1.5418 Å); θ the Bragg angle; β is the pure diffraction broadening of a peak at half-height, i.e., the broadening due to the crystallite dimensions. The size of nanoparticles calculated by the Scherrer formula from Fig. 3a, b are 30 and 33 nm, respectively.

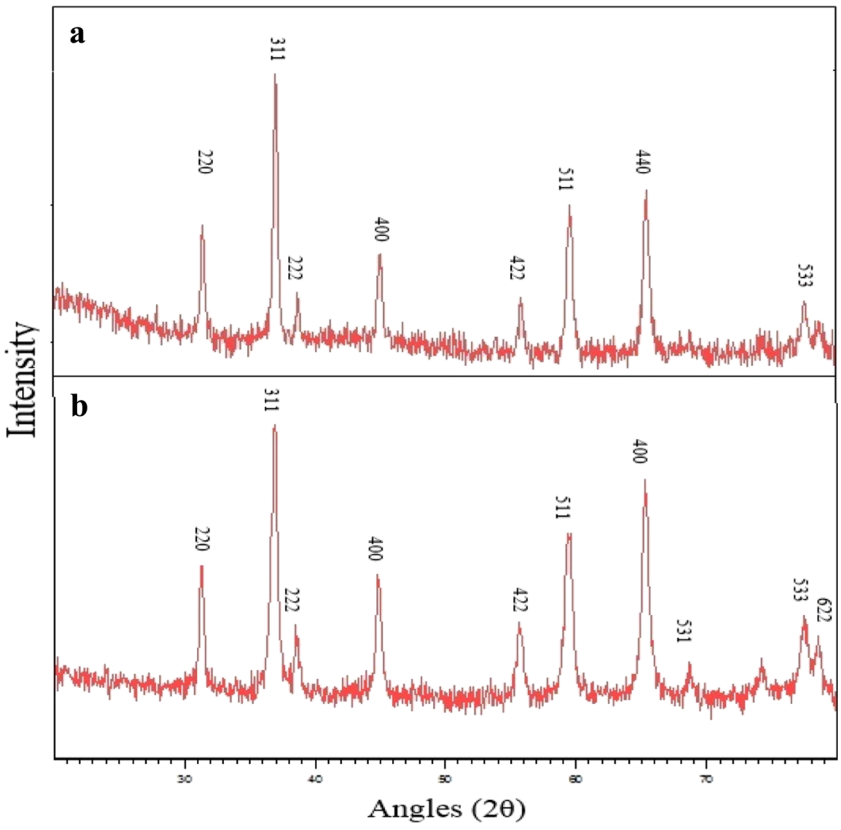

Fig. 3 XRD pattern of Co_3O_4 showing peak indices and 2θ positions, **a** for **1** and **b** for **2**

FE-SEM Morphological Analysis of Co_3O_4 Nanoparticles

The morphology of cobalt oxide nanoparticles was examined by FE-SEM (Fig. 4). Figure 4a, b is the low and high magnification pictures of Co_3O_4 nanoparticles obtained from thermal decomposition of [Co^{II}(bqbenzo)]. These nanoparticles are agglomerated and polymorphic, with a nonuniform distribution of sizes and shape. The Co_3O_4 nanoparticles obtained from thermal decomposition of [Co^{II}(bqb)] precursor, however, are mostly crystalline with a narrow shape and size distribution forming chains of well ordered nanoparticles (Fig. 4 c, d). The FE-SEM image shows that the mean particle size of Co_3O_4 nanoparticles obtained from [Co^{II}(bqb)] is below 45 nm. These nanoparticles show remarkable electrocatalytic activity in oxygen evolution reaction (OER) (*vide infra*).

Electrochemical Evaluation in OER

Figure 5 shows the CV of Co_3O_4 (**1**) and Co_3O_4 (**2**) catalysts in 1 M KOH at room temperature. The observed single anodic peak and corresponding cathodic peak in the potential window of 500–550 mV are due to Co(IV)/Co(III) redox reaction (1) [35, 36]:

$$CoOOH + OH^- \rightarrow CoO_2 + H_2O + e^-$$

The surface of the oxide film changes partially to the hydrated CoOOH phase according to the following reaction (2) [37].

$$Co_3O_4 + H_2O + OH^- \rightarrow 3CoOOH + e^-$$

As evident from Fig. 5, the Co_3O_4 (**2**) has more intense anodic and cathodic redox peaks which can be related to the

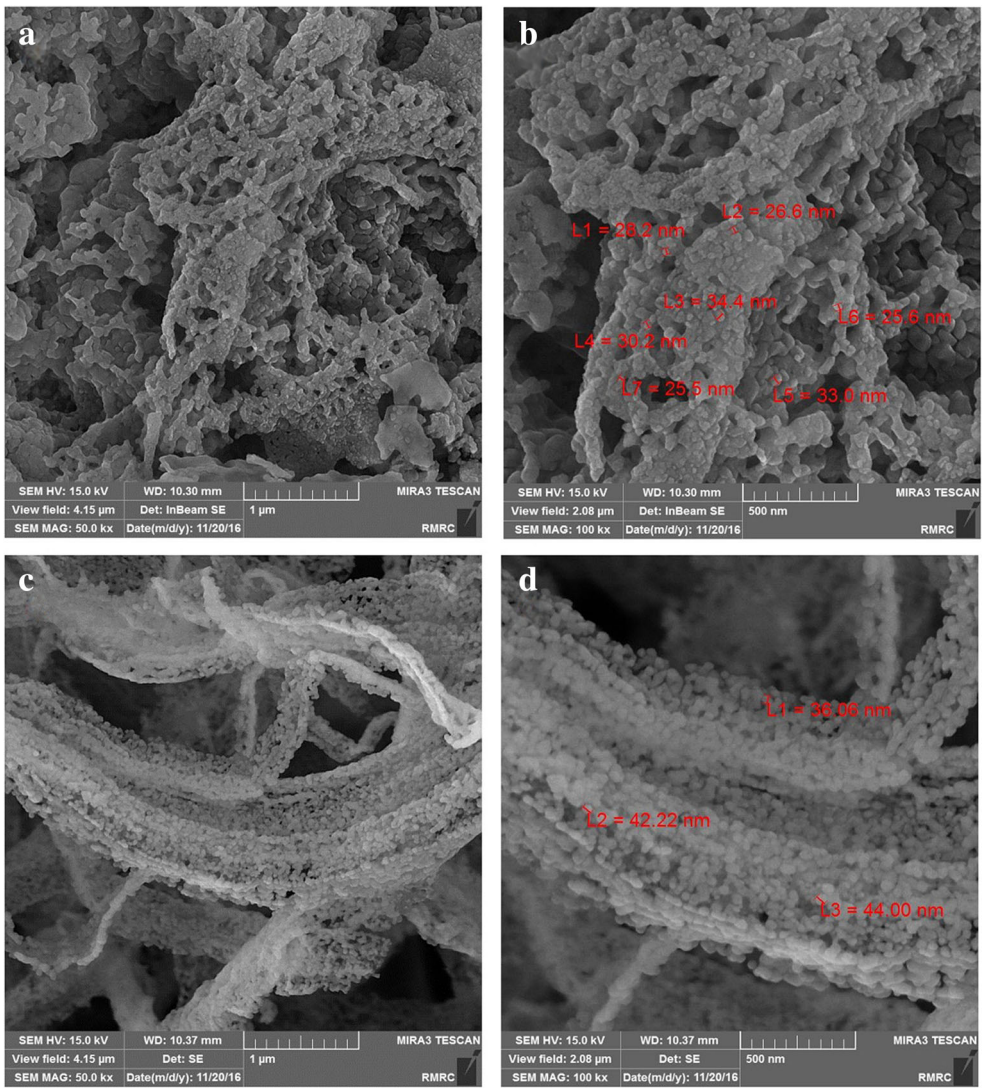

Fig. 4 The FE-SEM images of Co_3O_4 nanoparticles, **1** and **2**, obtained from thermal decomposition of [Co^{II}(bqbenzo)] (**a**, **b**) and [Co^{II}(bqb)] (**c**, **d**), respectively

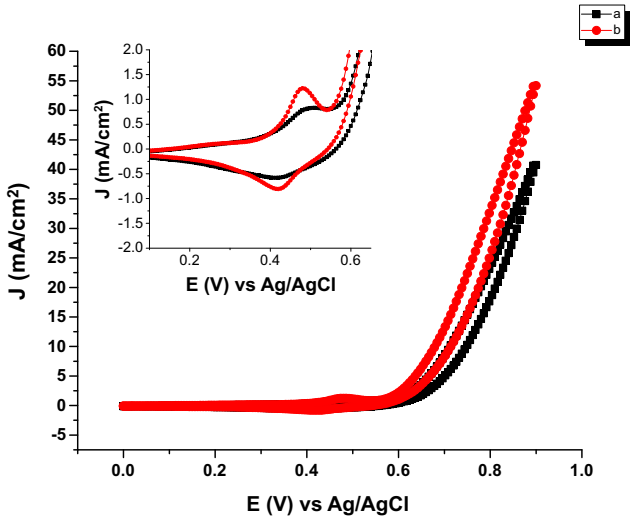

Fig. 5 CV of (*a*) Co_3O_4 (**1**) and (*b*) Co_3O_4 (**2**) recorded at room temperature in 1 M KOH with a sweep rate 50 mV/s. The *inset image* shows details at a high magnification

higher activity of Co_3O_4 (**2**) in OER as compared to Co_3O_4 (**1**) (inset in Fig. 5). These results are consistent with those obtained from morphological investigation.

The stability of the Co_3O_4 (**1**) and Co_3O_4 (**2**) electrodes were checked by taking consecutive cyclic voltammograms in 1 M KOH and the results are presented in Fig. 6a, b. The resulting data after 500 cycles indicate that Co_3O_4 (**1**) has a notable stability during catalyst aging process in OER (Fig. 6a), compared to Co_3O_4 (**2**) with 48% current loss at 0.8 V. The higher stability of Co_3O_4 (**1**) is presumably due to the more robust polymorphic structure of **1**, relative to **2**.

The catalytic activity of Co_3O_4 (**1**) and Co_3O_4 (**2**) was also studied by LSV and Tafel plot in 1 M KOH at room temperature. As shown in Fig. 7a, Co_3O_4 (**1**) and Co_3O_4 (**2**) have higher catalytic activity comparing to 10 wt% Pt/C and show lower onset potential and higher obtained current densities at 0.8 V. Moreover, the Tafel slope for Co_3O_4 (**1**) is lower than Co_3O_4 (**2**), i.e., 78 versus 84 mV dec^{-1}, respectively. These results indicate that the oxides surface enhances the OER remarkably, which is consistent with the obtained results in the literatures [38, 39]. Therefore, it could be concluded that Co_3O_4 (**1**) is a promising candidate anode catalyst for alkaline water electrolyzer.

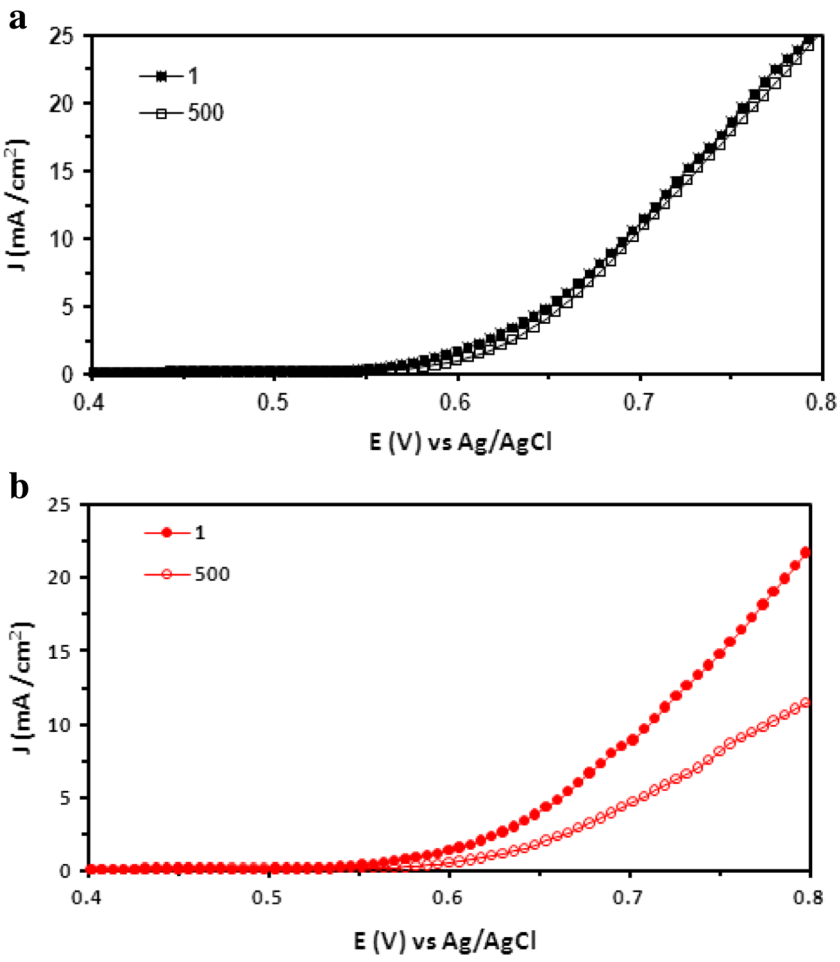

Fig. 6 LSV of **a** Co_3O_4 (**1**) and b Co_3O_4 (**2**) electrodes in 1 M KOH at 1 and, after 500 CV scans between 0.2 and 0.9 V, with the scan rate of 50 mV s^{-1}

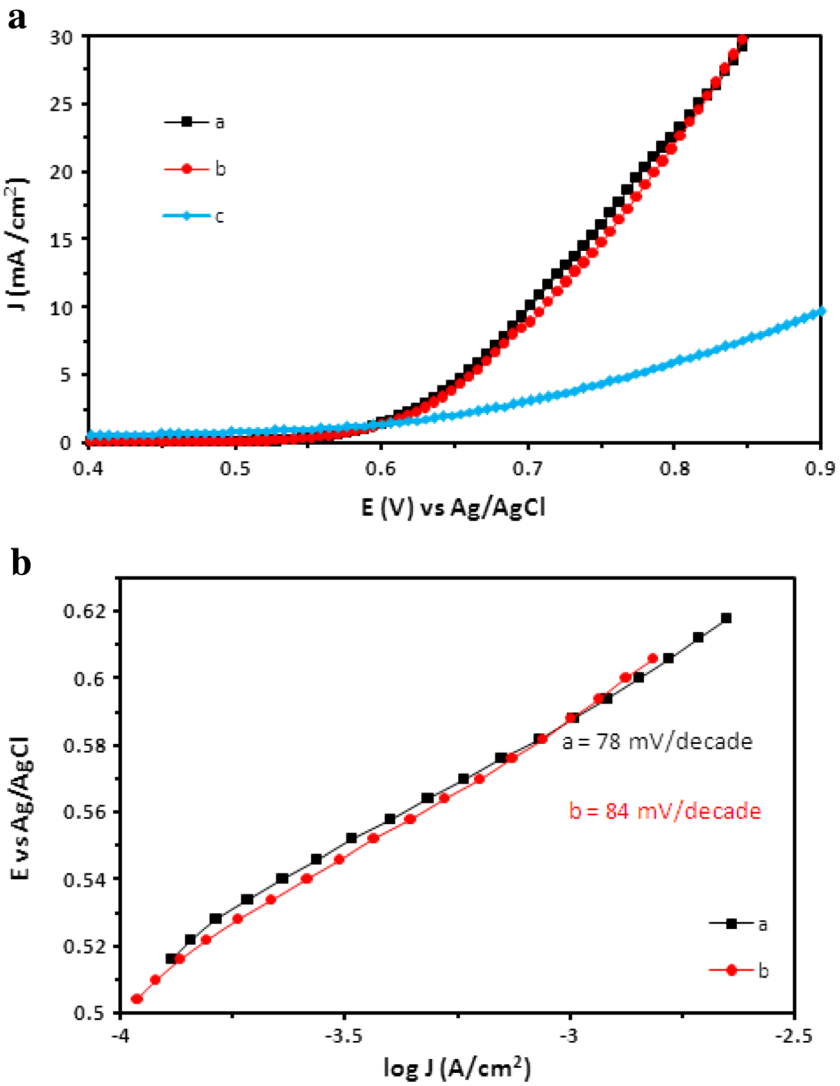

Fig. 7 **a** LSV of (*a*) Co_3O_4 (**1**), (*b*) Co_3O_4 (**2**), and (*c*) 10 wt% Pt/C at 5 mV s^{-1} in 1 M KOH. (**b**) Corresponding Tafel plots for OER on (*a*) Co_3O_4 (**1**) and (*b*) Co_3O_4 (**2**)

Conclusion

Co_3O_4 nanoparticles have been synthesized by the thermal decomposition of [Co^{II}(bqbenzo)] and [Co^{II}(bqb)]. The proposed method for the synthesis of Co_3O_4 nanoparticles is simple, mild, and inexpensive, making it promising and suitable for large scale synthesis of nanostructured cobalt oxide. Furthermore, the effect of benzoyl substituent on the morphology and nanoparticle size has been investigated by XRD and FE-SEM. While the Co_3O_4(**1**) nanoparticles obtained from thermal decomposition of [Co^{II}(bqbenzo)] are agglomerated and polymorphic, the Co_3O_4 (**2**) nanoparticles obtained from thermal decomposition of [Co^{II}(bqb)] precursor are mostly crystalline with a narrow shape and size distribution forming chains of well-ordered nanoparticles. The FE-SEM image shows that the mean particle size of Co_3O_4 (**2**) nanoparticles obtained from [Co^{II}(bqb)] are below 45 nm. The electrocatalytic activity of both oxides has been investigated by CV and LSV in an alkaline medium. Compared to the conventional Pt/C 10 wt% catalyst, both cobalt oxides **1** and **2** exhibit pronounced activities in OER in alkaline medium. The aging test results of both oxides reveal that Co_3O_4 (**1**) has an acceptable activity and stability during OER. Overall, the Co_3O_4 (**1**) shows a remarkable performance which can be considered as a promising catalyst for OER in alkaline water electrolysis.

Acknowledgements Partial support of this work by the Isfahan University of Technology Research Council and the Iranian Nano Technology Initiative Council is gratefully acknowledged.

References

1. P. Du, R. Eisenberg, Catalysts made of earth-abundant elements (Co, Ni, Fe) for water splitting: recent progress and future challenges. Energy Environ. Sci. **5**, 6012–6021 (2012)
2. L. Trotochaud, J. K. Ranney, K. N. Williams, S. W. Boettcher, Solution-cast metal oxide thin film electrocatalysts for oxygen evolution. J. Am. Chem. Soc. **134**, 17253–17261 (2012)

3. S. M. Barnett, K. I. Goldberg, J. M. Mayer, A soluble copper-bipyridine water-oxidation electrocatalyst. Nat. Chem. **4**, 498–502 (2012)
4. M. Garcia-Mota, M. Bajdich, V. Viswanathan, A. Vojvodic, A. T. Bell, J. K. Norskov, Importance of correlation in determining electrocatalytic oxygen evolution activity on cobalt oxides. J. Phys. Chem. **C116**, 21077–21082 (2012)
5. L. Duan, F. Bozoglian, S. Mandal, B. Stewart, T. Privalov, A. Llobet, L. Sun, A molecular ruthenium catalyst with water-oxidation activity comparable to that of photosystem II. Nat. Chem. **4**, 418–423 (2012)
6. Y. Surendranath, M. W. Kanan, D. G. Nocera, Mechanistic studies of the oxygen evolution reaction by a cobalt-phosphate catalyst at neutral *p*H. J. Am. Chem. Soc. **132**, 16501–16509 (2010)
7. M. G. Walter, E. L. Warren, J. R. McKone, S. W. Boettcher, Q. Mi, E. A. Santori, N. S. Lewis, Solar water splitting cells. Chem. Rev. **110**, 6446–6473 (2010)
8. Y. Lee, J. Suntivich, K. J. May, E. E. Perry, Y. Shao-Horn, Synthesis and activities of rutile IrO_2 and RuO_2 nanoparticles for oxygen evolution in acid and alkaline solutions. J. Phys. Chem. Lett. **3**, 399–404 (2012)
9. M. W. Louie, A. T. Bell, An investigation of thin-film Ni-Fe oxide catalysts for the electrochemical evolution of oxygen. J. Am. Chem. Soc. **135**, 12329–12337 (2013)
10. N. H. Chou, P. N. Ross, A. T. Bell, T. D. Tilley, Comparison of cobalt-based nanoparticles as electrocatalysts for water oxidation. ChemSusChem **4**, 1566–1569 (2011)
11. T. Maiyalagan, K. A. Jarvis, S. Therese, P. J. Ferreira, A. Manthiram, Spinel-type lithium 316 cobalt oxide as a bifunctional electrocatalyst for the oxygen evolution and oxygen 317 reduction reactions. Nat. Commun. **5**(3949), 1–8 (2014)
12. N. Suzuki, T. Horie, G. Kitahara, M. Murase, K. Shinozaki, Y. Morimoto, Novel noble-metal-free electrocatalyst for oxygen evolution reaction in acidic and alkaline media. Electrocatalysis **7**, 115–120 (2016)
13. M. Dincă, Y. Surendranath, D. G. Nocera, Nickel-borate oxygen-evolving catalyst that functions under benign conditions. Proc. Natl. Acad. Sci. **107**, 10337–10341 (2010)
14. K. Fominykh, J. M. Feckl, J. Sicklinger, M. Döblinger, S. Böcklein, J. Ziegler, L. Peter, J. Rathousky, E.-W. Scheidt, T. Bein, D. Fattakhova-Rohlfing, Ultrasmall dispersible crystalline nickel oxide nanoparticles as high-performance catalysts for electrochemical water splitting. Adv. Funct. Mater. **24**, 3123–3129 (2014)
15. H. Wang, H.-W. Lee, Y. Deng, Z. Lu, P.-C. Hsu, Y. Liu, D. Lin, Y. Cui, Bifunctional non-noble metal oxide nanoparticle electrocatalysts through lithium-induced conversion for overall water splitting. Nat. Commun. **6**(7261), 1–8 (2015)
16. R. K. Gupta, A. K. Sinha, B. N. Raja Sekhar, A. K. Srivastava, G. Singh, S. K. Deb, Synthesis and characterization of various phases of cobalt oxide nanoparticles using inorganic precursor. Appl. Phys. A Mater. Sci. Process. **103**, 13–19 (2011)
17. K. Thangavelu, K. Parameswari, K. Kuppusamy, Y. Haldorai, A simple and facile method to synthesize Co_3O_4 nanoparticles from metal benzoate dihydrazinate complex as a precursor. Mater. Lett. **65**, 1482–1484 (2011)
18. M. Goudarzi, M. Bazarganipour, M. Salavati-Niasari, Synthesis, characterization and degradation of organic dye over Co_3O_4 nanoparticles prepared from new binuclear complex precursors. RSC Adv**. 4**, 46517–46520 (2014)
19. O. Belda, C. Moberg, Bispyridylamides–coordination chemistry and applications in catalytic reactions. Coord. Chem. Rev. **249**, 727–740 (2005)
20. L. Yang, Z. Wu, L. Liang, X. Zhou, Synthesis, crystal structures and catalytic abilities of new macrocyclic bis-pyridineamido Mn^{III} and Fe^{III} complexes. J. Organomet. Chem. **694**, 2421–2426 (2009)
21. D. H. Lee, J. H. Lee, B. K. Park, E. Y. Kim, Y. Kim, C. Kim, I. M. Lee, High catalytic activities in the norbornene polymerization with neutral palladium complexes containing N4-type tetradentate chelating ligands. Inorg. Chim. Acta **362**, 5097–5102 (2009)
22. C. Y. Shi, E. J. Gao, S. Ma, M. L. Wang, Q. T. Liu, Synthesis, crystal structure, DNA-binding and cytotoxicity in vitro of novel cis-Pt(II) and trans-Pd(II) pyridine carboxamide complexes. Bioorg. Med. Chem. **20**, 7250–7254 (2010)
23. K. Sakai, H. Ozawa, H. Yamada, T. Tsubomura, M. Hara, A. Higuchi, M. A. Haga, A tris(2,2′-bipyridine)ruthenium(II) derivative tethered to a *cis*-$PtCl_2(amine)_2$ moiety: syntheses, spectroscopic properties, and visible-light-induced scission of DNA. J. Chem. Soc. Dalton Trans., 3300–3305 (2006)
24. R. D. Litto, V. Benessere, F. Ruffo, C. Moberg, Carbohydrate-based pyridine-2-carboxamides for Mo-catalyzed asymmetric allylic alkylations. Eur. J. Org. Chem., 1352–1356 (2009)
25. R. Ramachandran, P. Viswanathamurthi, Ruthenium(II) carbonyl complexes containing pyridine carboxamide ligands and PPh_3/$AsPh_3$/Py coligands: synthesis, spectral characterization, catalytic and antioxidant studies. Spectrochim. Acta Part A **103**, 53–61 (2013)
26. D. N. Lee, J. Y. Ryu, H. Kwak, Y. M. Lee, S. H. Lee, J. I. Poong, J. Lee, W. Shin, C. Kim, S. J. Kim, Y. Kim, Steric effect on construction of Cu(II) complexes with pyridine carboxamide ligands. J. Mol. Struct. **885**, 56–63 (2008)
27. A. A. Eroy-Reveles, Y. Leung, C. M. Beavers, M. M. Olmstead, P. K. Mascharak, Near-infrared light activated release of nitric oxide from designed photoactive manganese nitrosyls: strategy, design, and potential as NO donors. J. Am. Chem. Soc. **130**, 4447–4458 (2008)
28. H. A. Zamani, R. Kamjoo, M. Mohammadhosseini, M. Zaferoni, Z. Rafati, M. R. Ganjali, Farnoush Faridbod, Soraia Meghdadi, Europium(III) PVC membrane sensor based on N-pyridine-2-carboxamido-8-aminoquinoline as a sensing material. Mater. Sci. Eng. C **32**, 447–451 (2012)
29. S. Meghdadi, K. Mereiter, M. Amirnasr, F. Karimi, A. Amiri, Synthesis, crystal structure and electrochemistry of cobalt(III) carboxamide complexes with amine and azide ancillary ligands. Polyhedron **68**, 60–69 (2014)
30. S. Meghdadi, M. Amirnasr, A. Amiri, Z. Musavizadeh Mobarakeh, Z. Azarkamanzad, Benign synthesis of N-(8-quinolyl pyridine-2-carboxamide) ligand (Hbpq), and its Ni(II) and Cu(II) complexes. A fluorescent probe for direct detection of nitric oxide in acetonitrile solution based on Hbpq copper(II) acetate interaction. C. R. Chim **17**, 477–483 (2014)
31. S. Meghdadi, M. Amirnasr, A. Amiri, Z. Azarkamanzad, K. Schenk Joβ, F. Fadaee, A. Amiri, S. Abbasi, Benign synthesis of the unsymmetrical ligand N-(quinolin-8-yl) pyrazine-2-carboxamide. Preparation, electrochemistry, antibacterial activity, and crystal structures of Cu(II) and Zn(II) complexes. J. Coord. Chem. **66**, 4330–4343 (2013)
32. M. Salavati-Niasari, F. Davar, M. Mazaheri, M. Shaterian, Preparation of cobalt nanoparticles from [bis(salicylidene)cobalt(II)]–oleylamine complex by thermal decomposition. J. Magn. Magn. Mater. **320**, 575–578 (2008)
33. M. Herrero, P. Benito, F. M. Labajos, V. Rives, Nanosize cobalt oxide-containing catalysts obtained through microwave-assisted methods. Catal. Today **128**, 129–137 (2007)
34. R. Jenkins, R. L. Snyder, *Chemical analysis: introduction to X-ray powder diffractometry* (Wiley, Inc., New York, 1996), p. 90
35. X. Wu, K. Scott, A Li-doped Co_3O_4 oxygen evolution catalyst for nonprecious metal alkaline anion exchange membrane water electrolysers. Int. J. Hydrogen Energ. **38**, 3123–3129 (2013)
36. B. Chi, H. Lin, J. Li, Cations distribution of $CuxCo_3$-xO_4 and its electrocatalytic activities for oxygen evolution reaction. Int. J. Hydrogen Energ. **33**, 4763–4768 (2008)
37. M. Hamdani, R. N. Singh, P. Chartier, Co_3O_4 and Co-based spinel oxides bifunctional oxygen electrodes. Int. J. Electrochem. Sci. **5**, 556–577 (2010)

38. Y.-C. Liu, J. A. Kza, J. A. Switzer, Conversion of electrodeposited Co(OH) to CoOOH and Co_3O_4, and comparison of their catalytic activity for the oxygen evolution reaction. Electrochim. Acta **140**, 359–365 (2014)

39. Y. Liang, Y. Li, H. Wang, J. Zhou, J. Wang, T. Regier, H. Dai, Co_3O_4 nanocrystals on graphene as a synergistic catalyst for oxygen reduction reaction. Nature Mater. **10**, 780–786 (2011)